Nanoscale imaging of RNA with expansion microscopy

Fei Chen[1–3,10], Asmamaw T Wassie[1–3,10], Allison J Cote[4], Anubhav Sinha[5], Shahar Alon[2,3], Shoh Asano[2,3], Evan R Daugharthy[6,7], Jae-Byum Chang[2,3], Adam Marblestone[2,3], George M Church[6,8], Arjun Raj[4] & Edward S Boyden[1–3,9]

The ability to image RNA identity and location with nanoscale precision in intact tissues is of great interest for defining cell types and states in normal and pathological biological settings. Here, we present a strategy for expansion microscopy of RNA. We developed a small-molecule linker that enables RNA to be covalently attached to a swellable polyelectrolyte gel synthesized throughout a biological specimen. Then, postexpansion, fluorescent *in situ* hybridization (FISH) imaging of RNA can be performed with high yield and specificity as well as single-molecule precision in both cultured cells and intact brain tissue. Expansion FISH (ExFISH) separates RNAs and supports amplification of single-molecule signals (i.e., via hybridization chain reaction) as well as multiplexed RNA FISH readout. ExFISH thus enables super-resolution imaging of RNA structure and location with diffraction-limited microscopes in thick specimens, such as intact brain tissue and other tissues of importance to biology and medicine.

Nanoscale-resolution imaging of RNA throughout cells, tissues, and organs is key for understanding local RNA processing, for mapping structural roles of RNA, and for defining cell types and states. However, it has remained difficult to image RNA in intact tissues with the nanoscale precision required to pinpoint associations with cellular compartments or proteins important for RNA function. Recently, we developed an approach to physically magnify tissues, expansion microscopy (ExM)[1]. ExM isotropically magnifies tissues, enabling super-resolution imaging on conventional diffraction-limited microscopes. For example, ~4× linear expansion yields ~70-nm resolution using an ~300-nm diffraction-limited objective lens. In our original protocol, fluorophore tags were first targeted to proteins of interest via antibodies and then anchored to a swellable polyelectrolyte gel synthesized *in situ*. Isotropic expansion was subsequently achieved by proteolytic treatment to homogenize specimen mechanical properties followed by osmotic swelling of the specimen–gel composite.

Here, we have developed a small-molecule linker that enables RNA to be covalently attached to the ExM gel. We show that this procedure, which we call ExFISH, enables RNA FISH, which enables identification of transcripts *in situ* with single-molecule precision. In RNA FISH, a set of fluorescent probes complementary to a target strand of mRNA is delivered[2,3]. Single-molecule FISH (smFISH) can be performed with multiple fluorophores delivered to a single mRNA via oligonucleotide probes[4]. In intact tissues, amplification strategies, such as hybridization chain reaction (HCR)[5,6] and branched DNA amplification[7,8], can allow a large number of fluorophores to be targeted to a single mRNA. We show that ExFISH can support smFISH in cell culture and HCR-amplified FISH in intact mouse brain tissues. We demonstrate the power of ExFISH for revealing nanoscale structures of long noncoding RNAs (lncRNAs) as well as for localizing neural mRNAs to individual dendritic spines. ExFISH will be useful for a diversity of questions relating the structure and location of RNA to biological functions.

RESULTS

ExFISH, design and validation of RNA anchoring chemistry

We first determined a strategy for covalently linking RNAs directly to the ExM gel. Although transcripts are crosslinked to proteins during fixation, the strong proteolysis of ExM precludes a reliance on proteins for RNA retention (**Supplementary Fig. 1**). We thus reasoned that covalently securing RNA molecules directly to the ExM gel via a small-molecule linker would enable the interrogation of these molecules postexpansion. To achieve this aim, we synthesized a reagent from two building blocks: a molecule containing an amine as well as an alkylating group that primarily reacts to the *N7* of guanine and a molecule that contains an amine-reactive succinamide ester and a polymerizable acrylamide moiety. Commercially available reagents exist that satisfy each of these two profiles, such as Label-IT Amine (MirusBio) and 6-((acryloyl)amino)hexanoic acid (Acryloyl-X SE, here abbreviated AcX, Life Technologies; all reagents are listed in **Supplementary Table 1**). We named this molecule,

[1]Department of Biological Engineering, Massachusetts Institute of Technology, Cambridge, Massachusetts, USA. [2]Media Lab, Massachusetts Institute of Technology, Cambridge, Massachusetts, USA. [3]McGovern Institute, Massachusetts Institute of Technology, Cambridge, Massachusetts, USA. [4]Department of Bioengineering, University of Pennsylvania, Philadelphia, Pennsylvania, USA. [5]Division of Health Sciences and Technology, Massachusetts Institute of Technology, Cambridge, Massachusetts, USA. [6]Wyss Institute for Biologically Inspired Engineering, Boston, Massachusetts, USA. [7]Department of Systems Biology, Harvard Medical School, Boston, Massachusetts, USA. [8]Department of Genetics, Harvard Medical School, Boston, Massachusetts, USA. [9]Department of Brain and Cognitive Sciences, Massachusetts Institute of Technology, Cambridge, Massachusetts, USA. [10]These authors contributed equally to this work. Correspondence should be addressed to E.S.B. (esb@media.mit.edu).

RECEIVED 14 MARCH; ACCEPTED 18 MAY; PUBLISHED ONLINE 4 JULY 2016; DOI:10.1038/NMETH.3899

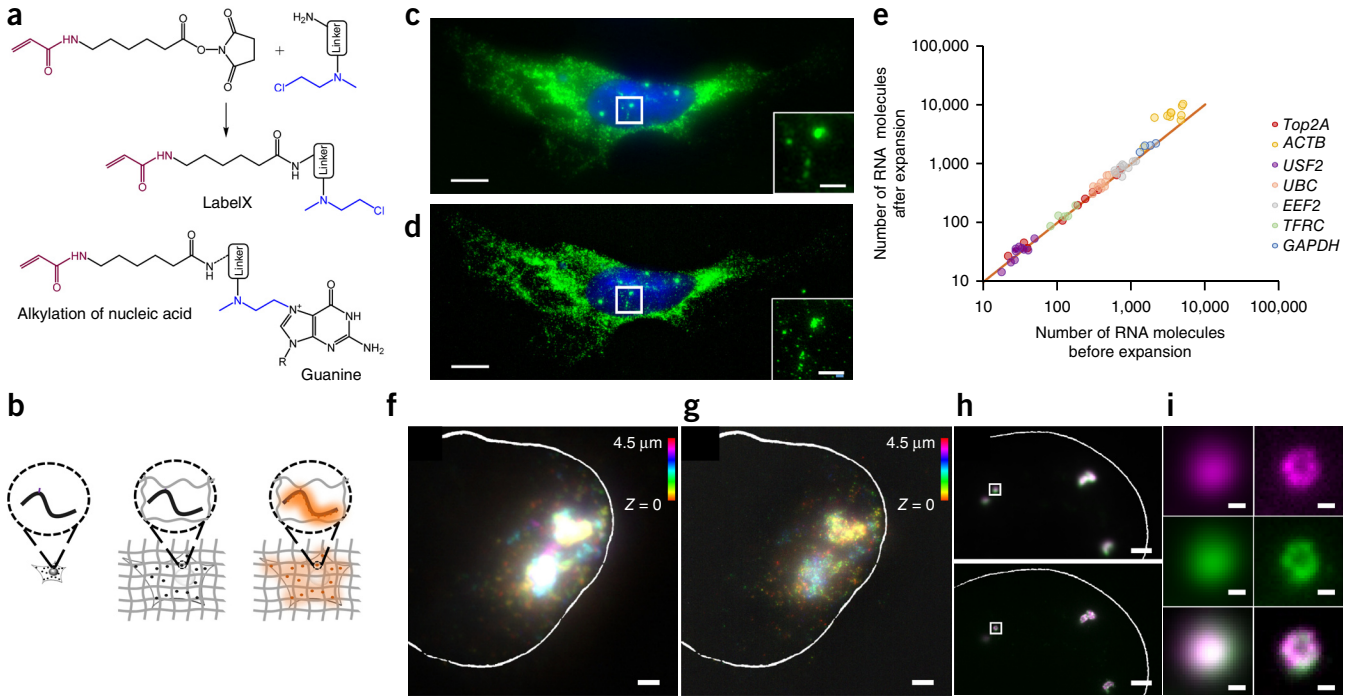

Figure 1 | Design and validation of ExFISH chemistry. (**a**) Acryloyl-X SE (top left) is reacted to Label-IT amine (top right) via NHS-ester chemistry to form LabelX (middle), which serves to make RNA gel anchorable by alkylating its bases (e.g., the N7 position of guanines) (bottom). (**b**) Workflow for ExFISH: biological specimens are treated with LabelX (left), which enables RNA to be anchored to the ExM gel (middle). Anchored RNA can be probed via hybridization (right) after gelation, digestion, and expansion. (**c**) smFISH image of *ACTB* before expansion of a cultured HeLa cell. Inset shows zoomed-in region, highlighting transcription sites in nucleus. (**d**) As in **c**, using ExFISH. (**e**) smFISH counts before versus after expansion for seven different transcripts (n = 59 cells; each symbol represents one cell). (**f**) smFISH image of XIST long non-coding RNA (lncRNA) in the nucleus of an HEK293 cell before expansion (white line denotes nuclear envelope in **f**–**h**). (**g**) As in **f**, using ExFISH. (**h**) smFISH image before expansion (top) and using ExFISH (bottom) of *NEAT1* lncRNA in the nucleus of a HeLa cell. Magenta and green indicate probesets binding to different parts of the 5′ (1–3, 756 nts) of *NEAT1* (see Online Methods). (**i**) Insets showing a *NEAT1* cluster (boxed region of **h**) with smFISH (left) and ExFISH (right). Scale bars (white, in pre-expansion units; blue scale bars are divided by the expansion factor noted); (**c**,**d**) 10 µm (expansion factor, 3.3×), inset 2 µm; (**f**,**g**) 2 µm (3.3×), Z scale represented by color coding in pre-expansion units; (**h**) 2 µm (3.3×); and (**i**) 200 nm (3.3×).

which enables RNA to be covalently functionalized with a free-radical polymerizable group, LabelX (**Fig. 1a**). We verified that LabelX does not impede smFISH readout (**Supplementary Fig. 2**). We then designed a procedure in which a sample could be treated with LabelX to make its RNAs gel anchorable, followed by gel formation, proteolysis, and osmotic swelling as performed in the original ExM protocol. Once a sample was thus expanded, the RNAs could then be interrogated through FISH (**Fig. 1b**).

To quantify RNA-transcript-anchoring yield after expansion, we used smFISH probes targeting mRNAs of varying copy number (seven targets, with copy number ranging from ~10 to ~10,000 per cell, n = 59 cells across all seven targets) in cultured HeLa cells. smFISH images, taken with probes delivered before (**Fig. 1c**) and after (**Fig. 1d**) expansion to the same cells, showed no loss of transcript detectability with expansion for both low- and high-copy-number transcripts (**Fig. 1e**). The ratio of transcripts detected was near unity at low transcript counts (for example, in the tens); however, more transcripts were detected after expansion for highly expressed mRNAs (for example, in the thousands) (**Supplementary Fig. 3** and **Supplementary Table 2**). This difference arose from the high density of smFISH spots for these targets in the unexpanded state, with the expansion process decrowding spots that were previously indistinguishable. For example, for smFISH against *ACTB*, we were able to resolve individual *ACTB* mRNA puncta postexpansion even within transcriptional foci in the nucleus (**Fig. 1c** versus **d**), which can be dense with mRNA on account of transcriptional bursting. Thus, ExFISH is capable of supporting single-molecule RNA readout in the expanded state. Since Label-IT also reacts to DNA, the ExFISH process enables uniform expansion of the nucleus (**Supplementary Fig. 4**). The isotropy of ExFISH (**Supplementary Fig. 5**) was numerically similar to that observed when protein targets were labeled and expanded in the original ExM protocol[1]. In recent ExM protocols in which proteins are anchored to the same hydrogel as used in ExFISH, with a similar linker[9,10], the distortion is small (a few percent distortion in cells and tissues). These earlier results, since they were obtained with similar polymer chemistry, serve to bound the ExFISH distortion. The expansion factor is slightly lower than in our original ExM paper (i.e., ~3.3× versus ~4×; expansion factors can be found in the figure legends of this manuscript) because of the salt required to support hybridization of probes.

Nanoscale imaging of lncRNA with ExFISH

We imaged lncRNAs known to serve structural roles in cell biology. We imaged the lncRNA XIST, whose role in inactivating the X chromosome may depend on initial association with specific chromatin subregions through a process that is still being revealed[11]. The pre-expansion image (**Fig. 1f**) shows two bright

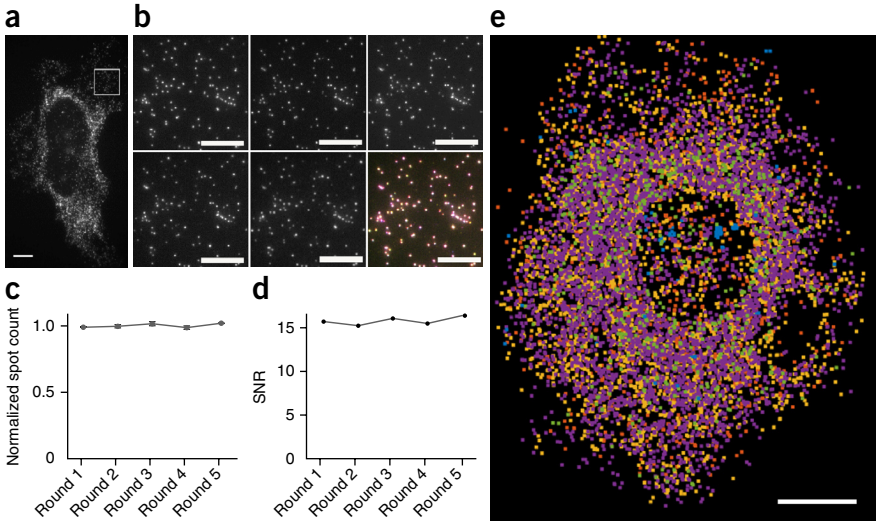

Figure 2 | Serially hybridized and multiplexed ExFISH. (**a**) Widefield fluorescence image of ExFISH targeting *GAPDH* in a cultured HeLa cell. (**b**) Boxed region of **a**, showing five repeated restainings following probe removal (see Online Methods); lower right panel shows an overlay of the five images (with each a different color, red, green, blue, magenta, or yellow), showing colocalization. (**c**) ExFISH RNA counts for each round, normalized to the round 1 count; plotted is mean ± standard error; $n = 3$ regions of **a**. (**d**) Signal-to-noise ratio (SNR) of ExFISH across the five rounds of staining of **a**, computed as the mean puncta brightness divided by the s.d. of the background. (**e**) Composite image showing ExFISH with serially delivered probes against six RNA targets in a cultured HeLa cell (raw images in **Supplementary Fig. 6**); colors are as follows: *NEAT1*, blue; *EEF2*, orange; *GAPDH*, yellow; *ACTB*, purple; *UBC*, green; *USF2*, light blue. Scale bars (expanded coordinates): (**a**) 20 µm; (**b**) 10 µm; and (**e**) 20 µm.

globular fluorescent regions, presumably corresponding to the X chromosomes of HEK cells undergoing inactivation[11–13], but postexpansion, individual puncta were apparent both within the globular regions as well as nearby (**Fig. 1g**). Additionally, we used ExFISH to examine the previously described[14] ring-shaped morphology of ensembles of *NEAT1* lncRNAs (**Fig. 1h**), which researchers have hypothesized play an important role in gene expression regulation and nuclear mRNA retention[15]. Before expansion, *NEAT1* presented in the form of bright, diffraction-limited puncta (**Fig. 1h**,**i**), but after expansion, the ring-shaped morphology became clear (**Fig. 1h**,**i**). Given the complex 3D structure of the genome[16], mapping lncRNAs may be useful in defining key chromatin regulatory complexes and their spatial configurations.

Super-resolved, multiplexed imaging of RNA with ExFISH

The combination of covalent RNA anchoring to the ExM gel and the decrowding of the local environment that results from expansion could facilitate strategies that have been proposed for multiplexed RNA readout[17–19] based upon sequential hybridization with multiple probe sets. In order to facilitate multiple cycles of FISH, we re-embedded expanded specimens in charge-neutral polyacrylamide. This process allowed expanded gels to be immobilized for multiround imaging and additionally stabilized the expanded specimen throughout salt concentration changes in the protocol. Such re-embedded samples exhibited similar expansion factors as non-re-embedded samples (i.e., ~3×), and they were robust to multiple wash–stain cycles as assessed by repeated application of the same probe set (**Fig. 2a**; **Supplementary Fig. 6**, showing five rounds of smFISH staining against *GAPDH* on cultured cells). This stability was observed even under stringent wash conditions designed to minimize cycle-to-cycle crosstalk (for example, 100% formamide). Across the five rounds, there was no distortion of the locations of individual RNA spots from round to round (**Fig. 2b**), nor variance in detection efficiency or signal-to-noise ratio (**Fig. 2c**,**d**). Having validated the cycle-to-cycle consistency, we next demonstrated the capability of multiplexed ExFISH by applying probes for *GAPDH*, *UBC*, *NEAT1*, *USF2*, *ACTB*, and *EEF2* in series, enabling six individual RNAs to be identified and localized in the same cell (**Fig. 2e** and **Supplementary Fig. 6**). Thus, serial FISH is applicable to samples expanded after securing RNA to the swellable polymer as here described, making it straightforward to apply probe sets computationally designed to yield more information per FISH cycle, such as MERFISH[18–20].

3D nanoscale imaging of RNA in mouse brain tissue

ExM allows for facile super-resolution imaging of thick 3D specimens such as brain tissue on conventional microscopy hardware[1]. We applied ExFISH to samples of Thy1–YFP mouse brain tissue[21], using the YFP protein to delineate neural morphology (**Fig. 3a**,**b**). Endogenous YFP protein was anchored to the polyacrylate gel via AcX using the proExM protocol[9], and RNA was anchored via LabelX. Since smFISH yields signals too dim to visualize in intact tissues using confocal imaging, we applied the previously described technique of HCR[5], in particular the next-generation DNA HCR amplifier architecture[6] (schematic in **Supplementary Fig. 7**). In samples containing mouse cortical and hippocampal regions, mRNAs for YFP (**Fig. 3c**) and glutamic acid decarboxylase 1 (*Gad1*) (**Fig. 3d**) were easily visualized using a widefield microscope, with YFP mRNA well localized to YFP-fluorescing cells (**Fig. 3e**) and *Gad1* mRNA localized to a population of cells with characteristic arrangement throughout specific layers of the cortex and hippocampus[22]. Examining brain specimens at high magnification using a confocal spinning-disk microscope revealed that individual transcripts could be distinguished because of the physical magnification of ExM (**Fig. 3f**, with YFP and *Gad1* mRNA highlighted), with even highly overexpressed transcripts (e.g., YFP) cleanly resolved into individual puncta (**Fig. 3f**). When FISH probes were omitted, minimal background HCR amplification was observed (**Supplementary Fig. 8**). Given that ExM enables super-resolution imaging on diffraction-limited microscopes, which can be scaled to very fast imaging speeds[23], we used a commercially available lightsheet microscope on a Thy1–YFP brain slice to enable visualization of multiple transcripts with single-molecule precision throughout a volume ~575 × 575 × 160 µm

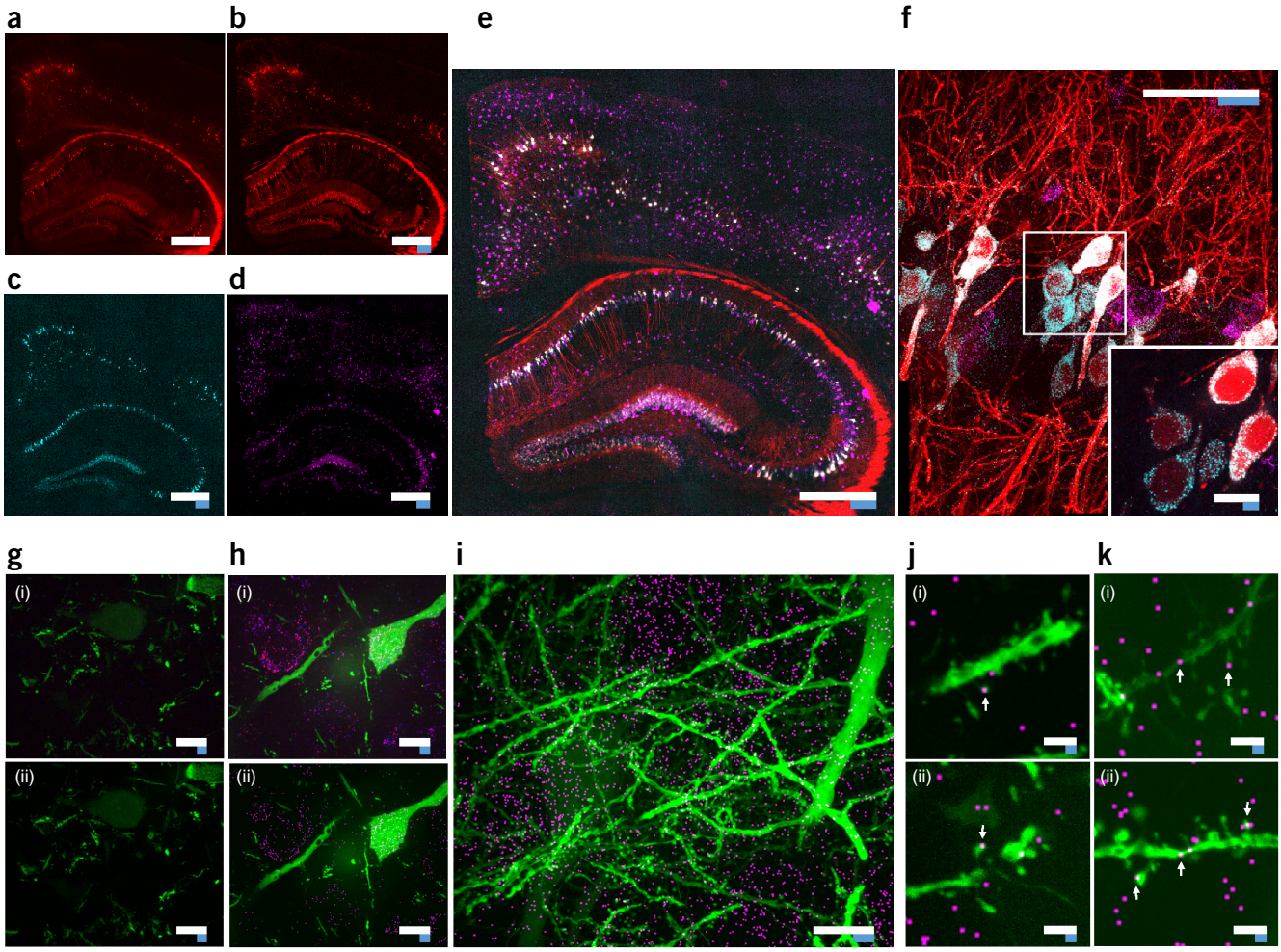

Figure 3 | Nanoscale imaging of RNA in mammalian brain. (**a**) Widefield fluorescence image of Thy1–YFP mouse brain. (**b**) Postexpansion widefield image of **a**. (**c**) Widefield fluorescence showing HCR-ExFISH of YFP mRNA in the sample of **b**. (**d**) As in **c**, but for *Gad1* mRNA. (**e**) Composite of **b**–**d**, highlighting distribution of *Gad1* versus Thy1–YFP mRNAs. (**f**) Confocal image of mouse hippocampal tissue from **e**, showing single RNA puncta. Inset, one plane of the boxed region (red, YFP protein; cyan, YFP mRNA; magenta, *Gad1* mRNA). (**g**) Confocal image (i) and processed image (ii) of HCR-ExFISH using a missense *Dlg4* probe in Thy1–YFP mouse tissue (green, YFP protein). The raw image (i) uses alternating probes in two colors (red, *Dlg4* missense even; blue, *Dlg4* missense odd). The processed image (ii) shows zero colocalized spots (magenta). (**h**) As in **g**, but for HCR-ExFISH targeting *Actb* in Thy1–YFP mouse brain (green, YFP protein; red, *Actb* even; and blue, *Actb* odd in (i); colocalized spots in magenta (ii)). (**i**) Confocal image of hippocampal tissue showing colocalized *Dlg4* puncta (magenta) overlaid on YFP (green). (**j**) Dendrites with *Dlg4* mRNA localized to spines (arrows). (i), (ii), two representative examples. (**k**) As in **j**, but with HCR-ExFISH of *Camk2a* mRNA showing transcripts in dendritic spines and processes. (**i**–**k**) Magenta channel depicts colocalized puncta location. Raw images in **Supplementary Figure 10**. Scale bars (white, in pre-expansion units; blue scale bars are divided by the expansion factor noted): (**a**) 500 μm; (**b**–**e**) 500 μm (expansion factor 2.9×); (**f**) 50 μm (2.9×), inset 10 μm; (**g**–**i**) 10 μm (3×); (**j**,**k**) 2 μm (3×). (**e**,**i**) maximum-intensity projection (MIP) 27 μm thick (pre-expanded units); (**g**,**h**,**j**,**k**) MIPs ~1.6 μm thick.

thick in just 3 h (~6×10^{10} voxels in three colors; **Supplementary Fig. 9** and **Supplementary Video 1**).

HCR amplifies a target-binding event into a bright fluorescent signal (**Supplementary Fig. 7**). A stringent method for assessing detection accuracy is to label individual RNAs with different probe sets bearing different colors[24,25], which shows that 50–80% of mRNAs thus targeted will be doubly labeled when assessed in cell culture; a 50% colocalization is interpreted as $\sqrt{0.5}$ (~70%) detection efficiency (assuming probe independence); this is a lower bound as it excludes false positives. In order to assess the false-positive and false-negative rates for single-molecule visualization in expanded tissues, we delivered pairs of probe sets targeting the same transcript with different initiators. This scheme resulted in amplified fluorescent signals of two different colors from the same target (**Supplementary Fig. 10**), giving a measure of the hybridization efficiency. Delivering probe sets against a nonexistent transcript also gives a measure of false-positive rate. We delivered a probe set against a missense probe (*Dlg4* reversed, **Fig. 3g**) as well as a nonexistent transcript (mCherry, **Supplementary Table 3**), using Thy1–YFP mouse brain samples, and we found a low but nonzero spatial density of dim, yet amplified, puncta (1 per 61 μm^3 in unexpanded coordinates, *Dlg4* reversed; 1 per 48 μm^3, mCherry). Essentially zero of these puncta exhibited colocalization (0/1,209 spots, *Dlg4* reversed; 4/1,540 spots, mCherry). In contrast, when a transcript was present (*Actb*), a large fraction of the puncta exhibited colocalization (an average of 58% of probes in one color colocalized with other color, 15,866/27,504 spots; **Fig. 3h** and **Supplementary Table 3**),

indicative of a 75% detection efficiency, comparable to the non-amplified single-molecule studies described above.

We used two-color HCR ExFISH against mRNAs to image their position within cellular compartments such as dendritic spines, which require nanoscale resolution for accurate identification or segmentation. We probed the *Dlg4* mRNA, which encodes the prominent postsynaptic scaffolding protein PSD-95 and which is known to be dendritically enriched[7]. We obtained a degree of colocalization (53%; 5,174/9,795 spots) suggesting a high detection efficiency of 73% (**Fig. 3i**). We also probed the mRNA for *Camk2a*, finding a detection efficiency of 78% (colocalization, 61%; 8,799/14,440 spots; **Supplementary Fig. 10**). We focused on puncta that were colocalized, thus suppressing false-positive errors and giving a lower bound on transcript detection (**Supplementary Fig. 10**). Focusing on individual dendrites in these expanded samples revealed that individual *Dlg4* (**Fig. 3j**) and *Camk2a* (**Fig. 3k**) mRNAs could indeed be detected in a sparse subset of dendritic spines as well as in fine dendritic processes. To facilitate multiplexed HCR readout, we developed modified HCR hairpins that can be disassembled using toe-hold mediated strand displacement[26] (**Supplementary Fig. 11**). These modified HCR amplifiers enable multiple cycles of HCR by disassembling the HCR polymer between subsequent cycles. Given that neurons can have tens of thousands of synapses and mRNAs can have low copy number, the ability to map mRNAs at synapses throughout neuronal arbors may be useful for a diversity of questions in neuroscience ranging from plasticity to development to degeneration.

DISCUSSION

We present a novel reagent, easily synthesized from commercial precursors, that enables RNA to be covalently anchored for expansion microscopy. The resulting procedure, ExFISH, enables RNAs to be probed through single-molecule FISH labeling as well as HCR amplification. We validated RNA retention before versus after expansion, finding excellent yield and decrowding of RNAs for more accurate RNA counts and localization. This enabled us to visualize, with nanoscale precision and single-molecule resolution, RNA structures such as XIST and NEAT1, lncRNAs whose emergent structure has direct implications for their biological roles. The anchoring was robust enough to support serial smFISH, including repeated washing and probe hybridization steps and multiplexed readout of RNA identity and location, implying that using probes designed according to specific coding strategies[17–19] would support combinatorial multiplexing, in which each additional cycle yields exponentially more transcript information. The covalent anchoring of RNA to the ExM gel may also support enzymatic reactions to be performed in expanded samples such as reverse transcription, rolling-circle amplification (RCA), fluorescent *in situ* sequencing (FISSEQ)[27], and other strategies for transcriptomic readout or SNP detection[28], within intact samples.

ExM, being a physical form of magnification, enables nanoscale resolution even on conventional diffraction-limited microscopes. Expanding samples makes them transparent and homogeneous in index of refraction, in part because of the volumetric dilution and in part because of washout of nonanchored components[1]. Thus, strategies combining ExM with fast diffraction-limited methods like lightsheet microscopy[23] may result in 'best of both worlds' performance metrics: the voxel sizes of classical super-resolution methods but the voxel acquisition rates of increasingly fast diffraction-limited microscopes[1]. The decrowding of RNAs enables another key advantage: reducing the effective size of the self-assembled amplification product of HCR, which we here applied to enable nanoscale-resolution visualization of RNA in intact tissues; the Pierce lab is developing optimized single-molecule HCR strategies[29], although the results here shown follow the protocols of refs. 5 and 6. An HCR amplicon of size 500 nm in the postexpanded sample would, because of the greater distance between RNAs, have an effective size of 500/3.5 = ~150 nm. The lower packing density of amplicons facilitates the imaging of more transcripts per experiment[19] with nanoscale precision. Other methods of achieving brighter signals may be possible. For example, brighter fluorophores such as quantum dots[30] or bottlebrush fluorophores[31] could, in principle, obviate the need for signal amplification. The expanded state may enable better delivery of these and other bulky fluorophores into samples. Other amplification strategies may be possible as well, including enzymatic (e.g., RCA[28], tyramide amplification[22], and HRP amplification) as well as nonenzymatic (e.g., branched DNA) methods, although reaction efficiency and diffusion of reagents into the sample must be considered.

ExFISH may find many uses in neuroscience and other biological fields. In the brain, for example, RNA is known to be trafficked to specific synapses as a function of local synaptic activity[32] and intron content[33], it is known to be locally translated[7,34,35], and the presence and translation of axonal RNAs remains under investigation[36]. We anticipate that, coupled with straightforward multiplexed coding schemes, this method could be used for transcriptomic profiling of neuronal cell types *in situ* as well as for the super-resolved characterization of neuronal connectivity and synaptic organization in intact brain circuits, key to an integrative understanding of the mechanisms underlying neural circuit function and dysfunction. More broadly, visualizing RNAs within cells and their relationship with RNA processing and trafficking machinery may reveal new insights throughout biology and medicine.

METHODS

Methods and any associated references are available in the online version of the paper.

Note: Any Supplementary Information and Source Data files are available in the online version of the paper.

ACKNOWLEDGMENTS

Lightsheet imaging was performed in the W.M. Keck Facility for Biological Imaging at the Whitehead Institute for Biomedical Research. We would like to acknowledge W. Salmon for assistance with the Zeiss Z.1 lightsheet, S. Olenych from Carl Zeiss Microscopy for providing the microscopy filters, and H.T. Choi and N. Pierce for advice and consultation on HCR. E.R.D. is supported by NIH CEGS grant P50 HG005550, NIH CEGS grant 1 RM1 HG008525, and NSF GRF grant DGE1144152. A.T.W. acknowledges the Hertz Foundation Fellowship. F.C. acknowledges the NSF Fellowship and Poitras Fellowship. AR and AC acknowledge support from NIH/NHLBI grant 1U01HL129998. E.S.B. acknowledges support by the New York Stem Cell Foundation–Robertson Award, NSF CBET 1053233, MIT Media Lab Consortium, the MIT Synthetic Intelligence Project, NIH Director's Pioneer Award 1DP1NS087724, NIH 2R01DA029639, NIH Director's Transformative Award 1R01MH103910, NIH 1R24MH106075, IARPA D16PC00008, the Open Philanthropy Project, and Jeremy and Joyce Wertheimer. J.-B.C. was supported by a Simons Postdoctoral Fellowship.

AUTHOR CONTRIBUTIONS

F.C., A.T.W., E.R.D., A.M., G.M.C., and E.S.B. conceived RNA-tethering strategies to the ExM gel. F.C. and A.T.W. conceived and developed the LabelX reagent.

F.C., A.T.W., J.-B.C., and S. Alon developed ExM gel stabilization by re-embedding. F.C., A.T.W., and E.R.D. conceived and developed reversible HCR strategies. F.C., A.T.W., and E.S.B. designed, and F.C. and A.T.W. performed experiments. A.J.C. and A.R. provided FISH reagents and guidance on usage, and A.J.C. performed experiments. A.S. performed data analysis. S. Asano performed lightsheet imaging and analysis. E.S.B. supervised the project. F.C., A.T.W., A.S., and E.S.B. wrote the paper, and all authors contributed edits and revisions.

COMPETING FINANCIAL INTERESTS

The authors declare competing financial interests: details are available in the online version of the paper.

1. Chen, F., Tillberg, P.W. & Boyden, E.S. Optical imaging. Expansion microscopy. *Science* **347**, 543–548 (2015).
2. Femino, A.M., Fay, F.S., Fogarty, K. & Singer, R.H. Visualization of single RNA transcripts *in situ*. *Science* **280**, 585–590 (1998).
3. Levsky, J.M. & Singer, R.H. Fluorescence *in situ* hybridization: past, present and future. *J. Cell Sci.* **116**, 2833–2838 (2003).
4. Raj, A., van den Bogaard, P., Rifkin, S.A., van Oudenaarden, A. & Tyagi, S. Imaging individual mRNA molecules using multiple singly labeled probes. *Nat. Methods* **5**, 877–879 (2008).
5. Choi, H.M.T. *et al.* Programmable *in situ* amplification for multiplexed imaging of mRNA expression. *Nat. Biotechnol.* **28**, 1208–1212 (2010).
6. Choi, H.M.T., Beck, V.A. & Pierce, N.A. Next-generation *in situ* hybridization chain reaction: higher gain, lower cost, greater durability. *ACS Nano* **8**, 4284–4294 (2014).
7. Cajigas, I.J. *et al.* The local transcriptome in the synaptic neuropil revealed by deep sequencing and high-resolution imaging. *Neuron* **74**, 453–466 (2012).
8. Wang, F. *et al.* RNAscope: a novel *in situ* RNA analysis platform for formalin-fixed, paraffin-embedded tissues. *J. Mol. Diagn.* **14**, 22–29 (2012).
9. Tillberg, P.W. *et al.* Expansion microscopy of biological specimens with protein retention. *Nat. Biotechnol.* doi:10.1038/nbt.3625 (2016).
10. Chozinski, T.J. *et al.* Expansion microscopy with conventional antibodies and fluorescent proteins. *Nat. Methods* **13**, 485–488 (2016).
11. Engreitz, J.M. *et al.* The Xist lncRNA exploits three-dimensional genome architecture to spread across the X chromosome. *Science* **341**, 1237973 (2013).
12. Panning, B., Dausman, J. & Jaenisch, R. X chromosome inactivation is mediated by Xist RNA stabilization. *Cell* **90**, 907–916 (1997).
13. Plath, K., Mlynarczyk-Evans, S., Nusinow, D.A. & Panning, B. Xist RNA and the mechanism of X chromosome inactivation. *Annu. Rev. Genet.* **36**, 233–278 (2002).
14. Mito, M., Kawaguchi, T., Hirose, T. & Nakagawa, S. Simultaneous multicolor detection of RNA and proteins using super-resolution microscopy. *Methods* **98**, 158–165 (2015).
15. Clemson, C.M. *et al.* An architectural role for a nuclear noncoding RNA: NEAT1 RNA is essential for the structure of paraspeckles. *Mol. Cell* **33**, 717–726 (2009).
16. Lieberman-Aiden, E. *et al.* Comprehensive mapping of long-range interactions reveals folding principles of the human genome. *Science* **326**, 289–293 (2009).
17. Lubeck, E. & Cai, L. Single-cell systems biology by super-resolution imaging and combinatorial labeling. *Nat. Methods* **9**, 743–748 (2012).
18. Lubeck, E., Coskun, A.F., Zhiyentayev, T., Ahmad, M. & Cai, L. Single-cell *in situ* RNA profiling by sequential hybridization. *Nat. Methods* **11**, 360–361 (2014).
19. Chen, K.H., Boettiger, A.N., Moffitt, J.R., Wang, S. & Zhuang, X. RNA imaging. Spatially resolved, highly multiplexed RNA profiling in single cells. *Science* **348**, aaa6090 (2015).
20. Beliveau, B.J. *et al.* Versatile design and synthesis platform for visualizing genomes with Oligopaint FISH probes. *Proc. Natl. Acad. Sci. USA* **109**, 21301–21306 (2012).
21. Feng, G. *et al.* Imaging neuronal subsets in transgenic mice expressing multiple spectral variants of GFP. *Neuron* **28**, 41–51 (2000).
22. Lein, E.S. *et al.* Genome-wide atlas of gene expression in the adult mouse brain. *Nature* **445**, 168–176 (2007).
23. Huisken, J., Swoger, J., Del Bene, F., Wittbrodt, J. & Stelzer, E.H.K. Optical sectioning deep inside live embryos by selective plane illumination microscopy. *Science* **305**, 1007–1009 (2004).
24. Batish, M., van den Bogaard, P., Kramer, F.R. & Tyagi, S. Neuronal mRNAs travel singly into dendrites. *Proc. Natl. Acad. Sci. USA* **109**, 4645–4650 (2012).
25. Cabili, M.N. *et al.* Localization and abundance analysis of human lncRNAs at single-cell and single-molecule resolution. *Genome Biol.* **16**, 20 (2015).
26. Zhang, D.Y. & Seelig, G. Dynamic DNA nanotechnology using strand-displacement reactions. *Nat. Chem.* **3**, 103–113 (2011).
27. Lee, J.H. *et al.* Highly multiplexed subcellular RNA sequencing *in situ*. *Science* **343**, 1360–1363 (2014).
28. Ke, R. *et al.* *In situ* sequencing for RNA analysis in preserved tissue and cells. *Nat. Methods* **10**, 857–860 (2013).
29. Shah, S. *et al.* Single-molecule RNA detection at depth via hybridization chain reaction and tissue hydrogel embedding and clearing. *Development* (in the press).
30. Bruchez, M. *et al.* Semiconductor nanocrystals as fluorescent biological labels. *Science* **281**, 2013–2016 (1998).
31. Fouz, M.F. *et al.* Bright fluorescent nanotags from bottlebrush polymers with DNA-tipped bristles. *ACS Cent. Sci.* **1**, 431–438 (2015).
32. Steward, O., Wallace, C.S., Lyford, G.L. & Worley, P.F. Synaptic activation causes the mRNA for the IEG Arc to localize selectively near activated postsynaptic sites on dendrites. *Neuron* **21**, 741–751 (1998).
33. Buckley, P.T. *et al.* Cytoplasmic intron sequence-retaining transcripts can be dendritically targeted via ID element retrotransposons. *Neuron* **69**, 877–884 (2011).
34. Steward, O. & Schuman, E.M. Compartmentalized synthesis and degradation of proteins in neurons. *Neuron* **40**, 347–359 (2003).
35. Buxbaum, A.R., Wu, B. & Singer, R.H. Single β-actin mRNA detection in neurons reveals a mechanism for regulating its translatability. *Science* **343**, 419–422 (2014).
36. Jung, H., Yoon, B.C. & Holt, C.E. Axonal mRNA localization and local protein synthesis in nervous system assembly, maintenance and repair. *Nat. Rev. Neurosci.* **13**, 308–324 (2012).

ONLINE METHODS

A table of all reagents and chemicals with part numbers and suppliers can be found in **Supplementary Table 1**.

Cell culture and fixation. HeLa (ATCC CCL-2) cells and HEK293-FT cells (Invitrogen) were cultured on Nunc Lab-Tek II Chambered Coverglass (Thermo Scientific) in D10 medium (Cellgro) supplemented with 10% fetal bovine serum (FBS) (Invitrogen), 1% penicillin–streptomycin (Cellgro), and 1% sodium pyruvate (BioWhittaker). Cells were authenticated by the manufacturer and tested for mycoplasma contamination to their standard levels of stringency and were here used because they are common cell lines for testing new tools. Cultured cells were washed once with DPBS (Cellgro), fixed with 10% formalin for 10 min, and washed twice with 1× PBS. Fixed cells were then stored in 70% ethanol at 4 °C until use.

Preparation of LabelX. Acryloyl-X, SE (6-((acryloyl)amino)hexanoic acid, succinimidyl ester, here abbreviated AcX; ThermoFisher) was resuspended in anhydrous DMSO at a concentration of 10 mg/mL, aliquoted, and stored frozen in a desiccated environment. Label-IT Amine Modifying Reagent (Mirus Bio, LLC) was resuspended in the provided Mirus Reconstitution Solution at 1 mg/ml and stored frozen in a desiccated environment. To prepare LabelX, 10 µL of AcX (10 mg/mL) was reacted with 100 µL of Label-IT Amine Modifying Reagent (1 mg/mL) overnight at room temperature with shaking. LabelX was subsequently stored frozen (–20 °C) in a desiccated environment until use.

Mouse perfusion. All methods for animal care and use were approved by the Massachusetts Institute of Technology Committee on Animal Care and were in accordance with the National Institutes of Health Guide for the Care and Use of Laboratory Animals. All solutions below were made up in 1× PBS prepared from nuclease-free reagents. Mice were anesthetized with isoflurane and perfused transcardially with ice-cold 4% paraformaldehyde. Brains were dissected out, left in 4% paraformaldehyde at 4 °C for one day, before moving to PBS containing 100 mM glycine. Slices (50 µm and 200 µm) were sliced on a vibratome (Leica VT1000S) and stored at 4 °C in PBS until use. The mouse used in **Figure 3** and related analyses was a Thy1–YFP (Tg(Thy1–YFP)16Jrs) male mouse in the age range 6–8 weeks. No sample-size estimate was performed, since the goal was to demonstrate a technology. No exclusion, randomization, or blinding of samples was performed.

LabelX treatment of cultured cells and brain slices. Fixed cells were washed twice with 1× PBS, once with 20 mM MOPS pH 7.7, and incubated with LabelX diluted to a desired final concentration in MOPS buffer (20 mM MOPS pH 7.7) at 37 °C overnight followed by two washes with 1× PBS. For cells, ranges of LabelX were used that resulted in a Label-IT Amine concentration of 0.006–0.02 mg/mL; higher concentrations resulted in somewhat dimmer smFISH staining (**Supplementary Fig. 12**), but otherwise no difference in staining quality was observed with Label-IT Amine concentrations in this range. For **Figure 1e** and **Supplementary Figures 1–3**, fixed cells were incubated with LabelX diluted to a final Label-IT Amine concentration of 0.02 mg/mL. For all other experiments in cells, fixed cells were treated with LabelX diluted to a final Label-IT Amine concentration of 0.006 mg/mL.

Brain slices, as prepared above, were incubated with 20 mM MOPS pH 7.7 for 30 min and subsequently incubated with LabelX diluted to a final Label-IT Amine concentration of 0.1 mg/mL (due to their increased thickness and increased fragmentation from formaldehyde postfixation) in MOPS buffer (20 mM MOPS pH 7.7) at 37 °C overnight. For YFP retention, slices were treated with 0.05 mg/mL AcX in PBS for >6 h at room temperature.

smFISH in fixed cultured cells before expansion. Fixed cells were briefly washed once with wash buffer (10% formamide, 2× SSC) and hybridized with RNA FISH probes in hybridization buffer (10% formamide, 10% dextran sulfate, 2× SSC) overnight at 37 °C. Following hybridization, samples were washed twice with wash buffer, 30 min per wash, and washed once with 1× PBS. Imaging was performed in 1× PBS.

smFISH probe sets targeting the human transcripts for *TFRC*, *ACTB*, *GAPDH*, *XIST*, and 5′ portion of *NEAT1* were ordered from Stellaris with Quasar 570 dye. Probe sets against *UBC*, *EEF2*, *USF2*, *TOP2A*, and full-length *NEAT1* were synthesized, conjugated to fluorophores, and subsequently purified by HPLC as described previously[37]. Oligonucleotide sequences for probe sets and accession numbers can be found in **Supplementary Table 4**.

Gelation, digestion, and expansion. Monomer solution (1× PBS, 2 M NaCl, 8.625% (w/w) sodium acrylate, 2.5% (w/w) acrylamide, 0.15% (w/w) *N*,*N*′-methylenebisacrylamide) was mixed, frozen in aliquots, and thawed before use. Monomer solution was cooled to 4 °C before use. For gelling cultured cells treated with LabelX, a concentrated stock of VA-044 (25% w/w, chosen instead of the ammonium persulfate (APS)/tetramethylethylenediamine (TEMED) of the original ExM protocol[1] because APS/TEMED resulted in autofluorescence that was small in magnitude but appreciable in the context of smFISH), was added to the monomer solution to a final concentration of 0.5% (w/w) and degassed in 200 µl aliquots for 15 min. Cells were briefly incubated with the monomer solution plus VA-044 and transferred to a humidified chamber. Subsequently, the humidified chamber was purged with nitrogen gas. To initiate gelation, the humidified chamber was transferred to a 60 °C incubator for two hours. For gelling brain slices treated with LabelX, gelation was performed as in the original ExM protocol (since, with HCR amplification, the slight autofluorescence of APS/TEMED was negligible). Gelled cultured cells and brain slices were digested with Proteinase K (New England BioLabs) diluted 1:100 to 8 units/mL in digestion buffer (50 mM Tris (pH 8), 1 mM EDTA, 0.5% Triton X-100, 500 mM NaCl), and digestion was carried out overnight at 37 °C. The gels expand slightly in the high osmolarity digestion buffer (~1.5×). After digestion, gels were stored in 1× PBS until use and expansion was carried out as previously described.

smFISH staining after expansion. Expanded gels were incubated with wash buffer (10% formamide, 2× SSC) for 30 min at room temperature and hybridized with RNA FISH probes in hybridization buffer (10% formamide, 10% dextran sulfate, 2× SSC) overnight at 37 °C. Following hybridization, samples were washed twice with wash buffer, 30 min per wash, and washed once with 1× PBS for another 30 min. Imaging was performed in 1× PBS.

Image processing and analysis of smFISH performed on cultured cells. Widefield images of smFISH staining performed before or after expansion were first processed using a rolling-ball background subtraction algorithm (FIJI)[38] with a 200 pixel radius. Subsequently, maximum-intensity *Z*-projections of these images were generated. Spots were then localized and counted using a code developed by the Raj lab and available online (http://rajlab.seas.upenn.edu/StarSearch/launch.html). This image analysis was performed for **Figures 1c–e** and **2a–c** and **Supplementary Figures 2–4**, **6**, and **8.**

Analysis of expansion isotropy. smFISH images before and after expansion of *TOP2A* were rigidly aligned via two control points using the FIJI plugin Turboreg[39]. Spots were localized and counted via a custom spot-counting Matlab code developed by the Raj lab (complete source code and instructions can be found at https://bitbucket.org/arjunrajlaboratory/rajlabimagetools/wiki/Home). Length measurements were performed among all pairs of points before expansion and the corresponding pairs of points after expansion via a custom Matlab script. Measurement error was defined as the absolute difference between the before and after expansion length measurements (**Supplementary Fig. 5c**).

Re-embedding of expanded gels in acrylamide matrix. For serial staining in cells, expanded gels were re-embeded in acrylamide to stabilize the gels in the expanded state. Briefly: gels were expanded in water and cut manually to ~1 mm thickness with a stainless steel blade. Cut gels were incubated in 3% acrylamide, 0.15% *N*,*N*′-methylenebisacrylamide with 0.05% APS, 0.05% TEMED, and 5 mM Tris pH 10.5 for 20 min on a shaker. There is an ~30% reduction in gel size during this step. Excess solution is removed from the gels and the gels are dried with light wicking from a laboratory wipe. Gels are placed on top of a bind-silane-treated (see below) coverslip or glass-bottom plate with a coverslip placed on top of the gels before moving into a container and purged with nitrogen. The container is moved to a 37 °C incubator for gelation for 1.5 h.

Staining of re-embedded gels. Re-embeded staining of gels was performed with exact conditions as described above for expanded gels, except posthybridization washes were replaced with two washes with wash buffer (10% formamide), 60 min per wash.

Probes were removed for multiple rounds of hybridization via treatment with DNAse I or 100% formamide. For DNAse I, samples were treated with DNAse I at 0.5 U/μL for 6 h at room temperature. For formamide stripping, samples were treated with 100% formamide at 6 h at 37 °C.

Bind-silane treatment of coverslips. Coverslips and glass-bottom 24-well plates were treated with bind-silane, a silanization reagent that incorporates acryloyl groups onto the surface of glass to perform in free-radical polymerization. Briefly, 5 μL of bind-silane reagent was diluted into 8 mL of ethanol, 1.8 mL of ddH_2O and 200 μL of acetic acid. Coverslips and glass-bottom 24-well plates were washed with ddH_2O, followed by 100% ethanol, followed by the diluted bind-silane reagent. After a brief wash with the diluted bind-silane reagent, the coverslip was dried, then washed with 100% ethanol, and then dried again. Coverslips were prepared immediately before use.

Probe design for HCR-FISH. Probe sequences and accession numbers for mRNA targets can be found in **Supplementary Table 4**. Probes were designed for HCR-FISH by tiling the CDS of mRNA targets with 22-mer oligos spaced by 3–7 bases. HCR initiators were appended to tiled sequences via a 2-base spacer (AA). For two-color probe-sets, even- and odd-tiled probes were assigned different HCR initiators to allow for amplification in different color channels.

RNA FISH with hybridization chain reaction amplification. Gelled samples were incubated with wash buffer (20% formamide, 2× SSC) for 30 min at room temperature and hybridized with HCR-initiator-tagged FISH probes in hybridization buffer (20% formamide, 10% dextran sulfate, 2× SSC) overnight at 37 °C. Following hybridization, samples were washed twice with wash buffer, 30 min per wash, and incubated with 1× PBS for 2 h at 37 °C. Subsequently, samples were incubated with 1× PBS for at least 6 h at room temperature. Before HCR amplification, hybridized samples were preincubated with amplification buffer (10% dextran sulfate, 5× SSC, 0.1% Tween 20) for 30 min. To initiate amplification, HCR hairpin stocks (Alexa 546 and Alexa 647 fluorophores) at 3 μM were snap-cooled by heating to 95 °C for 90 s and leaving to cool at room temperature for 30 min. Gelled samples were then incubated with HCR hairpins diluted to 60 nM in amplification buffer for 3 h at room temperature. After amplification, gels were washed with 5× SSCT (5× SSC, 0.1% Tween 20) twice with 1 h per wash.

Imaging of cultured cells using ExFISH. Both cultured cells as well as LabelX-treated and expanded cultured cells were imaged on a Nikon Ti-E epifluorescence microscope with a SPECTRA X light engine (Lumencor), and a 5.5 Zyla sCMOS camera (Andor), controlled by NIS-Elements AR software. For **Figure 1c**,**d** and **Supplementary Figures 3–5**, a 40 × 1.15 numerical aperture (NA) water-immersion objective was used. For all other experiments with cultured cells, a 60 × 1.4 NA oil-immersion objective was used.

For imaging smFISH probes labeled with fluorophores, the following filter cubes (Semrock, Rochester, NY) were used: Alexa 488, GFP-1828A-NTE-ZERO; Quasar 570, LF561-B-000; Alexa 594, FITC/TXRED-2X-B-NTE; and Atto 647N, Cy5-4040C-000.

Imaging of expanded brain slices. For epifluorescence imaging of brain sections before and after expansion (**Fig. 3a–e**) and to quantify expansion factors of tissue slices, specimens were imaged on a Nikon Ti-E epifluorescence microscope with a 4 × 0.2 NA air objective, a SPECTRA X light engine (Lumencor), and a 5.5 Zyla sCMOS camera (Andor), controlled by NIS-Elements AR software.

Postexpansion confocal imaging of expanded brain tissue was performed on an Andor spinning disk (CSU-X1 Yokogawa) confocal system with a 40 × 1.15 NA water objective (**Fig. 3f–k** and **Supplementary Fig. 10**) on a Nikon TI-E microscope body. GFP was excited with a 488 nm laser, with 525/40 emission filter. Alexa 546 HCR amplicons were excited with a 561 nm laser with 607/36 emission filter. Alexa 647 amplicons were excited with a 640 nm laser with 685/40 emission filter.

Gels were expanded in with three washes, 15 min each of 0.05 × SSC. The expansion factor can be controlled with the salt

doi:10.1038/nmeth.3899

concentration; we found that 0.05× SSC gives 3× expansion, while still giving enough salt for hybridization stability. To stabilize the gels against drift during imaging following expansion, gels were placed in glass-bottom 6-well plates with all excess liquid removed. If needed, liquid low-melt agarose (2% w/w) was pipetted around the gel and allowed to solidify to encase the gels before imaging.

Lightsheet imaging was performed on a Zeiss Z.1 lightsheet microscope. Briefly, the sample was fixed on a custom-made plastic holder using super glue and mounted on the freely rotating stage of the Z.1 lightsheet. Lightsheets were generated by two illumination objectives (5×, 0.1 NA), and the fluorescence signal detected by a 20× water-immersion objective (1.0 NA). Both lightsheets were used for data collection. The image volume dimensions of a single tile were 1,400 × 1,400 × 1,057 pixels, with a voxel size of 227 nm laterally and 469 nm axially. The laserlines used for excitation were 488 nm, 561 nm, and 638 nm. The individual laser transmissions were set to 5%, with the maximum output of 50 mW (488 nm and 561 nm) and 75 mW (638 nm). Optical filters used to separate and clean the fluorescence response included a Chroma T560lpxr as a dichroic and a Chroma 59001m for GFP and 59007m for Alexa 546 and Alexa 647. Two PCO.Edge 5.5m sCMOS cameras were used to capture two fluorescence channels simultaneously. Tiled data sets were taken with the Zeiss ZEN Software and subsequently merged and processed with FIJI, Arivis Vision4D, and Bitplane Imaris.

Two-color analysis in slices. A sliding window averaging (or minimization) scheme in *Z* (three optical sections) was used to suppress movement artifacts before spot-detection processing. RNA puncta were detected via a custom 3D spot-counting Matlab code developed by the Raj lab; complete source code and instructions can be found at https://bitbucket.org/arjunrajlaboratory/rajlabimagetools/wiki/Home.

Spot centroids were extracted from both color channels, and spots were determined to be colocalized if their centroids were within a 3 pixel radius in the *x*,*y* dimensions and a 2 pixel radius in the *z* dimension.

HCR reversal via toe-hold-mediated strand displacement. HCR amplification commences upon the addition of two HCR metastable amplifier hairpins. We designed a pair of HCR amplifiers, B2H1T and B2H2 (see below for sequence), where B2H1T bears a 6 bp toe-hold for strand displacement. To initiate HCR amplification, aliquots of these amplifiers at 3 μM were snap-cooled by heating to 95 °C for 90 s and leaving to cool at room temperature for 30 min. Gelled samples were then incubated with HCR hairpins diluted to 60 nM in amplification buffer for 3 h at room temperature. After amplification, gels were washed with 5× SSCT (5× SSC, 0.1% Tween 20) twice with 1 h per wash. Subsequently, HCR reversal was initiated by the addition of a displacement strand (see below for sequence) at 200 nM in 5× SSCT.

B2H1T:

GGCGGTTTACTGGATGATTGATGAGGATTTACGAG GAGCTCAGTCCATCCTCGTAAATCCTCATCAATCAT CAAATAG

B2H2:

/5′-ALEXA546-C12/ CCTCGTAAATCCTCATCAATC ATCCAGTAAACCGCCGATGATTGATGAGGATTTACGAG GATGGACTGAGCT

Displacement strand:

CTATTTGATGATTGATGAGGATTTACGAGGATG GACTGAGCT

37. Raj, A. & Tyagi, S. Detection of individual endogenous RNA transcripts *in situ* using multiple singly labeled probes. *Methods Enzymol.* **472**, 365–386 (2010).
38. Schindelin, J. *et al.* Fiji: an open-source platform for biological-image analysis. *Nat. Methods* **9**, 676–682 (2012).
39. Thévenaz, P., Ruttimann, U.E. & Unser, M. A pyramid approach to subpixel registration based on intensity. *IEEE Trans. Image Process.* **7**, 27–41 (1998).